Inorganic Chemistry

Article

pubs.acs.org/IC

On the Track to Silica-Supported Tungsten Oxo Metathesis Catalysts: Input from ^{17}O Solid-State NMR

Nicolas Merle,[†] Guillaume Girard,[‡] Nicolas Popoff,[†] Aimery De Mallmann,[†] Yassine Bouhoute,[†] Julien Trébosc,[‡] Elise Berrier,[‡] Jean-François Paul,[‡] Christopher P. Nicholas,[§] Iker Del Rosal,[⊥] Laurent Maron,*[,⊥] Régis M. Gauvin,*[,‡] Laurent Delevoye,*[,‡] and Mostafa Taoufik*[,†]

[†]Laboratoire de Chimie, Catalyse, Polymères et Procédés, UMR 5265 CNRS/ESCPE-Lyon/UCBL, ESCPE Lyon, F-308-43, Boulevard du 11 Novembre 1918, F-69616 Villeurbanne Cedex, France

[‡]Unité de Catalyse et de Chimie du Solide, CNRS UMR 8181, Université Lille Nord de France, F-59655 Villeneuve d'Ascq, France

[§]Exploratory Catalysis Research, UOP LLC, a Honeywell Company, 25 East Algonquin Road, Des Plaines, Illinois, United States

[⊥]Laboratoire de Physico-Chimie des Nano-Objets, CNRS UMR 5215, Université de Toulouse, INSA, UPS, 135 avenue de Rangueil, F-31077 Toulouse, France

Supporting Information

ABSTRACT: The grafting of an oxo chloro trisalkyl tungsten derivative on silica dehydroxylated at 700 °C was studied by several techniques that showed reaction via W−Cl cleavage, to afford a well-defined precatalyst for alkene metathesis. This was further confirmed by DFT calculations on the grafting process. ^{17}O labeling of the oxo moiety of a series of related molecular and supported tungsten oxo derivatives was achieved, and the corresponding ^{17}O MAS NMR spectra were recorded. Combined experimental and theoretical NMR studies yielded information on the local structure of the surface species. Assessment of the ^{17}O NMR parameters also confirmed the nature of the grafting pathway by ruling out other possible grafting schemes, thanks to highly characteristic anisotropic features arising from the quadrupolar and chemical shift interactions.

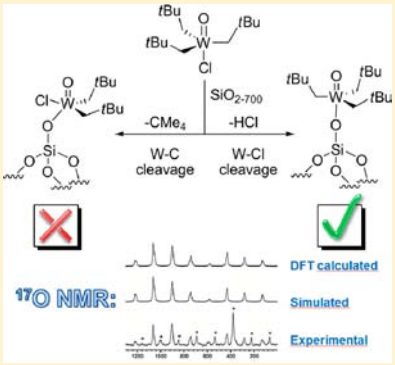

INTRODUCTION

Olefin metathesis holds a strategic position in modern chemical industry. Several commercial processes rely on this highly versatile reaction, such as the Olefin Conversion Technology (OCT) from ABB Lummus, or the Shell Higher Olefin Process (SHOP), which operate over a multimillion tons a year.[1] Classical catalytic systems involve transition metal (molybdenum, tungsten or rhenium) oxides supported on inorganic materials (silica, alumina, silica−alumina, etc.). For instance, tungsten oxide supported on silica is an efficient catalyst that has been used in industrial olefin metathesis processes since the 1960s.[2] From comparison with molecular systems, it is accepted that catalysis proceeds via surface metallacarbene species.[3] The nature of the active site is still a matter of debate but it seems clear that WO_3 crystallites are not involved in the catalytic cycle.[4] The catalytic activity is thus attributed to isolated tungsten surface species bearing a carbenic ligand. However, the concentration of such active sites in heterogeneous catalysts remains low.[5] Therefore, access to highly active heterogeneous catalysts that feature high concentration of metathesis-active centers is of major interest. Recently, we have disclosed the preparation of Lewis base-free oxo tetraalkyl tungsten complex **1** [$WONp_4$] (Np=CH_2tBu) using a specific alkylation procedure.[6] This species is closely related to the [$WONp_3X$] (X=Cl, Br, ONp) family described in the early 80s by Kress and Osborn.[7] Furthermore, in an attempt to bridge the gap between well-understood molecular catalysts and industrial formulations, we have proceeded to the grafting of **1** onto silica dehydroxylated at 700 °C to afford well-defined, supported oxo organometallic tungsten derivatives. As this material only features noninteracting silanols, it generates well-defined surface species [(≡SiO)$WONp_3$] **2** by protonolysis of the W−C bond by surface silanols (Scheme 1). This was shown by a combination of mass balance analysis and spectroscopic techniques (NMR, IR, Raman, EXAFS) supported by DFT calculations.

Very rewardingly, this catalytic material exhibited high activity in propene metathesis. Under dynamic conditions,

Scheme 1. Reaction of 1 with $SiO_{2\text{-}700}$

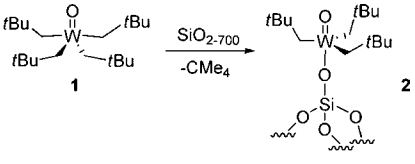

Received: June 17, 2013
Published: August 14, 2013

 © 2013 American Chemical Society dx.doi.org/10.1021/ic401521m | Inorg. Chem. 2013, 52, 10119−10130

the system reached 22 000 TON after 95 h, and only little decomposition was observed, in striking difference to the imido analogue.[8] These excellent performances motivated us to enhance the system. Indeed, one of the strengths of surface organometallic chemistry is the possibility to tune the active site structure by a careful choice of the organometallic precursor.[9] An attractive option to access highly active catalysts for olefin metathesis is the development of new organometallic oxo (surface) species that can be obtained from grafting of molecular precursors featuring varying coordination spheres around the tungsten center.

On the other hand, as we intend to prepare a series of organometallic (supported) oxo species, we needed to rely on a spectroscopic probe that will be directly connected to the active center, and thus reveal key-elements of its structure and electronic properties. This would help to achieve a better understanding of the synthesized species. We have recently shown that ^{17}O solid-state NMR is able to provide such an understanding.[10] ^{17}O being a quadrupolar nucleus (spin number I = 5/2), it provides information through isotropic chemical shift (CS), which spans over a wide range, and through anisotropic values such as chemical shift anisotropy (CSA) and quadrupolar coupling constant (C_Q), along with their respective asymmetry parameters (η). Such parameters are very sensitive to local and long distance interactions, and can provide unprecedented insight into the structure of supported catalysts.[10] This motivated us to address this issue by selectively labeling the oxo functionality of the complexes, which can bring further information on the structure of the active species and its initiation and deactivation steps. In this study dedicated to surface organometallic chemistry of tungsten oxo organometallic species, we will show that the structure of both the molecular and the supported oxo species can be better understood by relying on ^{17}O NMR coupled to DFT calculations.

RESULTS AND DISCUSSION

Study of the Reactivity of 3 with the Silica-Surface Model HOSi(O*t*Bu)$_3$. To expand the chemistry of supported tungsten oxo derivatives, we selected the readily available [$WONp_3Cl$] derivative **3**. This compound was first described by Kress and Osborn in the late 80s, and is obtained by trisalkylation of [$WOCl_4$].[7] It may have been expected that upon reaction with the surface, protonolysis of the W−C would occur similarly to what we observed for **1**, affording the bisalkyl oxo chloro derivative **4** (Scheme 2). However, a distinct reaction pathway could also consist of reaction through the W−Cl bond, releasing hydrochloric acid, and forming surface species **2**. In this case, the released HCl could also react with the organometallic species in the reaction mixture in a further step. Therefore, the selectivity of the grafting has to be determined, as several species could originate from the reaction of **3** with SiO_{2-700}.

Scheme 2. Possible Reaction Pathways of 3 with SiO_{2-700}

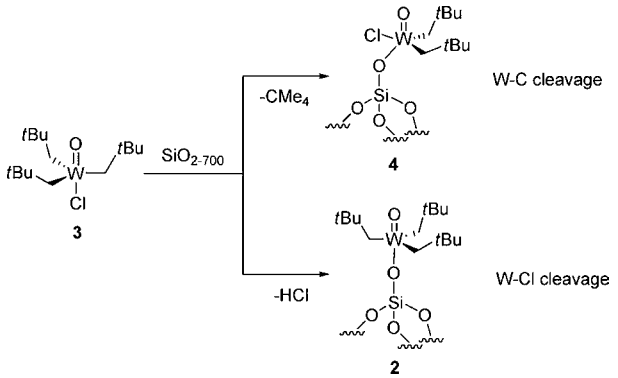

The reactivity of **3** with one equivalent of the HOSi(O*t*Bu)$_3$ silica-surface model[11] has been followed by solution NMR to determine the selectivity of the protonolysis of the W−C or W−Cl fragments by the silanol group (Figure 1).

No reaction is observed at room temperature after 1 h. However, upon heating at 60 °C for 10 min the ^1H NMR spectrum is consistent with a mixture of the starting materials and a new product featuring NMR signals typical for a complex with trigonal bipyramidal structure such as [{(*t*BuO)$_3$SiO}-$WONp_3$] (**5**), in which the oxo and alkoxide ligands are in mutually trans positions, similarly to previously reported complexes **3** and [(NpO)$WONp_3$].[7] Most particularly the methylenic fragment gives rise to a singlet at 2.19 ppm in ^1H NMR (with W-coupling satellites corresponding to $^2J_{W-H}$ = 12 Hz) and at 92.26 ppm in $^{13}C\{^1H\}$ NMR ($^1J_{W-C}$ = 93 Hz). No evolution of neopentane is observed by ^1H NMR, suggesting that the new product arises from the protonolysis of the W−Cl bond by the silanol group, and that cleavage of the W−C bond by either HOSi(O*t*Bu)$_3$ or HCl is not effective. After 1 h at 60 °C, the starting materials have been converted to 65% into **5**. However, upon cooling to room temperature, only 13% of this is observed because of the reverse reaction leading to **3** and HOSi(O*t*Bu)$_3$ in the presence of HCl (Scheme 3). Such reactivity is reminiscent of that of [$O(WONp_3)_2$] (**6**), which is in equilibrium with **3** upon reaction with HCl/Et_2O.[12] To reach full conversion, we have performed the reaction of **3** with (*t*BuO)$_3$SiOH in a Schlenk flask with a constant argon bubbling to remove the evolved HCl. This proceeds to the formation of **5** in 85% isolated yield. Several attempts at growing single crystals afforded colorless blocks of **5**, but disorder prevented full determination of the molecular structure by X-ray diffraction studies.

Grafting of 3 onto SiO_{2-700} and Characterization of the Resulting Material. Our preliminary investigations indicate that **3** reacts with a model of silica surface's silanols by W−Cl silanolysis with concomitant HCl production. This reaction is reversible, and is complete when the released hydrochloric acid is removed from the reaction mixture. The grafting of **3** was thus performed under dynamic vacuum, to shift the equilibrium toward formation of the surface species. In order to prepare a well-defined supported tungsten derivative, we resorted to the use of highly dehydroxylated silica that only bears noninteracting silanols.[9] Indeed, compound **3** reacts readily with silica dehydroxylated at 700 °C, to afford a colorless hybrid material. Infrared studies show quasi-quantitative consumption of the silanols (Figure 2).

Elemental analysis indicates a W and C% content of 4.02 and 4.02 wt %, respectively. This corresponds to a C/W molar ratio of 15.0. Furthermore, gas phase analysis reveals that the strongly major byproduct is HCl (223 μmol.g$(SiO_{2-700})^{-1}$, quantified by IR spectroscopy), while neopentane is only marginally produced (1.8 μmol.g$(SiO_{2-700})^{-1}$, quantified by GC). Thus, the characterization elements are in line with the formation of [(≡SiO)$WONp_3$] (**2**), just as in the case of the grafting of **1**. Furthermore, both the Raman spectrum (W═O band at 956 cm^{-1}, see Figure S1 in the Supporting Information) and the ^1H MAS and ^{13}C CP MAS NMR data

dx.doi.org/10.1021/ic401521m | Inorg. Chem. 2013, 52, 10119−10130

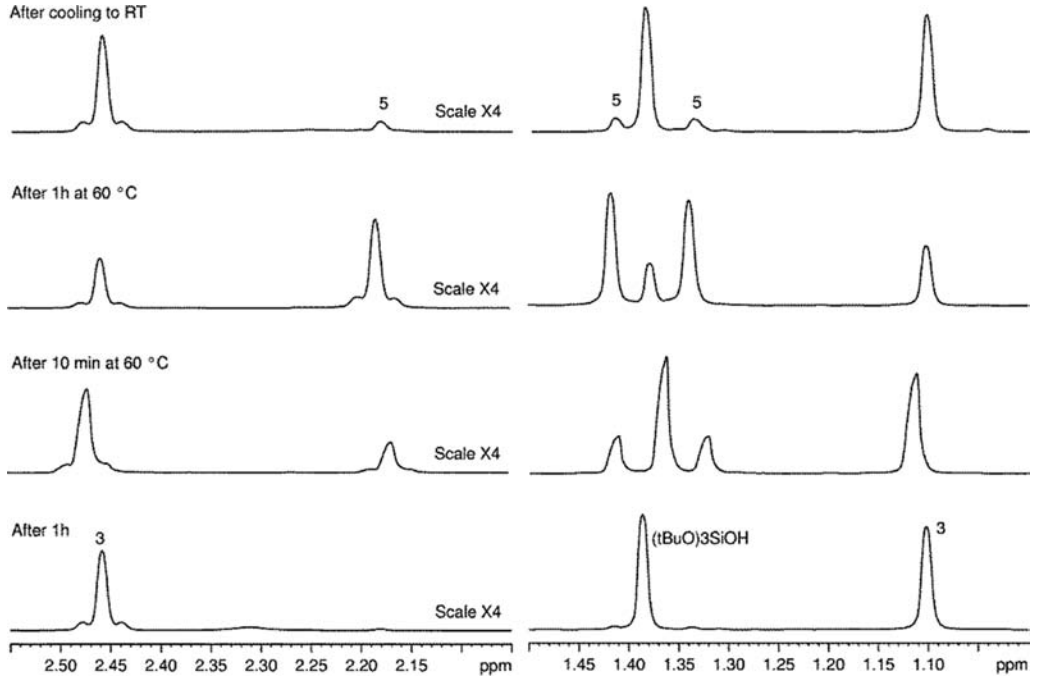

Figure 1. ^{1}H NMR follow-up of the reaction between **3** and HOSi(O*t*Bu)$_3$ (C_6D_6, 300 MHz).

Scheme 3. Formation of 5

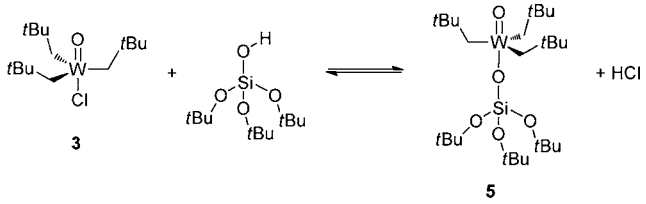

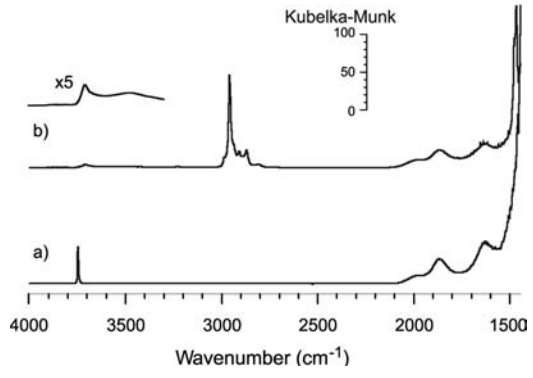

Figure 2. DRIFT spectra of (a) SiO_{2-700} and (b) **2**.

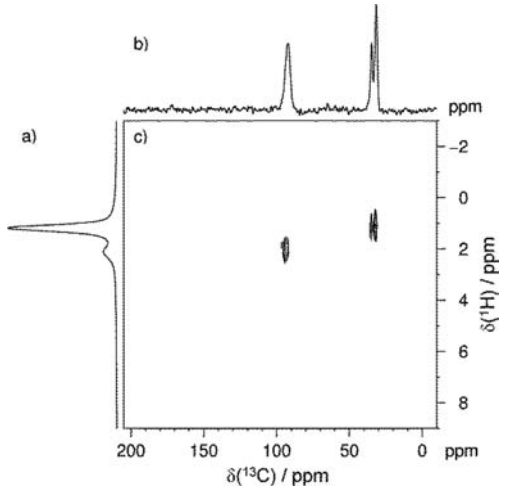

Figure 3. (a) ^{1}H, (b) ^{13}C CP, and (c) ^{1}H−^{13}C CP-HETCOR MAS NMR spectra of **2** (11.75T).

are in full agreement with such a conclusion. More specifically, the methylenic fragments give rise to ^{1}H and ^{13}C signals at 2.1 and 91 ppm, that strongly correlate in the HETCOR 2D spectrum (Figure 3).

These elements were supported by XAS studies. This consisted in recording and analyzing the W L_{III}-edge extended X-ray absorption fine structure (EXAFS) spectrum of both the molecular tungsten complex **3** and the supported species resulting from the grafting of **3** onto SiO_{2-700}, in order to refine their structures and compare them.

For **3** (Figure 4 and Table 1), the results are consistent with the following coordination sphere around W: one oxygen atom at 1.696(5) Å, assigned to an oxo ligand, three carbon at 2.11(1) Å, corresponding to σ-bonded carbon atoms of neopentyl ligands and one chloride at 2.43(1) Å. This is consistent with the bond distances found in the compound $[O(WONp_3)_2]$ (**6**) where the W=O (1.676−1.736 Å), and W−C (2.113−2.150 Å) bond lengths are in the same range.[12b] Similar W−Cl bond distances have been observed in $[W^{VI}OClX_3]$ type complexes: 2.397 and 2.427 Å for (μ^2-oxo)-bis(benzoyltrifluoroacetonato)-dichloro-oxo-tungsten(VI) (with a 1.696 Å W=O bond length),[13] 2.434(2) and 2.432(2) Å for $[WO\{N(iPr)Ar\}_2Cl_2]$ (with a 1.691(8) Å W=O bond length),[14] and 2.4212(2) Å for $[WO(C_6H_{12}O_2)(C_6H_{13}O_2)Cl]$ (with a 1.716(3) Å W=O bond length).[15] Similar parameters were obtained when fitting the $k^2\chi(k)$ spectrum. Furthermore, the fit was improved when considering a further layer of three C atoms backscatterers at 3.27(3) Å, assigned to the quaternary carbons of the neopentyl ligands. (this corresponds to a 126 ± 8° W−C−C angle, in agreement with the (123.7−127.4°)

dx.doi.org/10.1021/ic401521m | *Inorg. Chem.* 2013, 52, 10119−10130

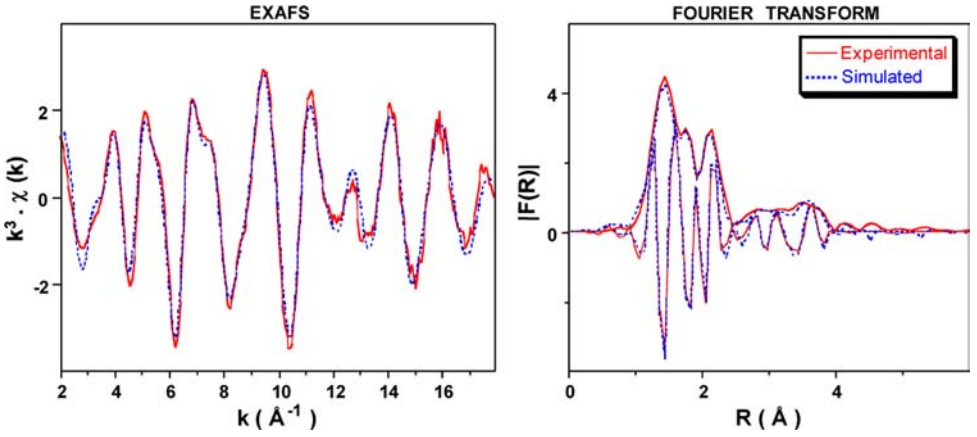

Figure 4. Tungsten L_{III}-edge k^3-weighted EXAFS (left) and corresponding Fourier transform (right, modulus, and imaginary part) with comparison to simulated curves for the molecular complex [$WONp_3Cl$], **3**. Solid lines, experimental; dashed lines, spherical wave theory.

Table 1. EXAFS Parameters for Molecular Complex 3[a,b]

type of neighbor	no. of neighbors	distance (Å)	σ^2 (Å^2)
W═O	1	1.696(5)	0.0016(4)
W-CH_2CMe_3	3	2.11(1)	0.0031(4)
W-Cl	1	2.43(1)	0.0039(8)
W-CH_2CMe_3	3	3.28(3)	0.006(4)
MS_{3l} O═W−Cl[c]	2	4.11(3)	0.003(2)
MS_{4l} O═W−Cl[c]	2	4.11[d]	0.03(2)

[a]The errors generated by the EXAFS fitting program "RoundMidnight" are indicated in parentheses. [b]Δk: [2.0−17.9 Å^{-1}] − ΔR: [0.7−4.1 Å] ([0.7−2.4 Å], when considering only the first coordination sphere); S_0^2 = 0.94; ΔE_0 = 8.7 ± 2.1 eV (the same for all shells); Fit residue: ρ = 4.9%; Quality factor: $(\Delta\chi)^2/\nu$ = 3.63 (ν = 24/36). $([(\Delta\chi)^2/\nu]_1$ = 8.1 with ν = 10/19, considering only the first coordination sphere with variation of the coordination numbers). [c]These two multiple scattering pathways (three and four legs) have been considered in the fit, assuming a geometry close to linearity between these three atoms.[7a,12b] [d]Shell constrained to the parameter above.

range found for **6**[12b]) and two multiple scattering O═W−Cl pathways corresponding to a quasi linear arrangement of these three atoms in the complex (trans configuration), as it was proposed by Osborn et al. on the basis of their NMR results.[7a]

For the species resulting from the grafting of **3** onto SiO_{2-700} (Figure 5), the disappearance of the direct W−Cl and multiple (O═W−Cl) scattering pathways can be clearly observed from the comparison of the moduli of the Fourier transforms of both molecular and supported species (contribution of the Cl backscatterer at ca. 2.1 Å and of the multiple scattering pathways at ca. 3.7 Å on the right part of Figure 5). The parameters extracted from the fit of the EXAFS spectrum (Table 2) are in fact quite similar to those published for [(≡SiO)$WONp_3$],[6] and are consistent with one oxo ligand at 1.703(5) Å, ca. one oxygen at 1.98(2) Å and three carbon atoms at 2.11(1) Å, respectively assigned to a siloxide and three neopentyl ligands, consistently with the bond distances found in **6** (see above). The rather long W−O distance found for this ≡SiO−W bond may indicate that the oxo and siloxy ligands are trans to each other in the surface complex. Similar parameters were obtained when fitting $k^1\chi(k)$ and $k^2\chi(k)$ spectra. The fit was also improved by adding two layers of backscatterers, one composed of three carbon atoms at 3.28(3) Å, attributed to the quaternary carbons of the neopentyl ligand and another one with ca. one silicon atom at 3.54(5) Å, assigned to a silicon of a surface siloxide ligand. Most noteworthy, these data are fully in line with those of the material obtained by [$WONp_4$] grafting.[6]

From these combined spectroscopic and analytical elements, and as observed for the molecular model reaction, the reaction of **3** with the silica surface does not proceed by W−C cleavage, but by W−Cl silanolysis and concomitant HCl release (Scheme

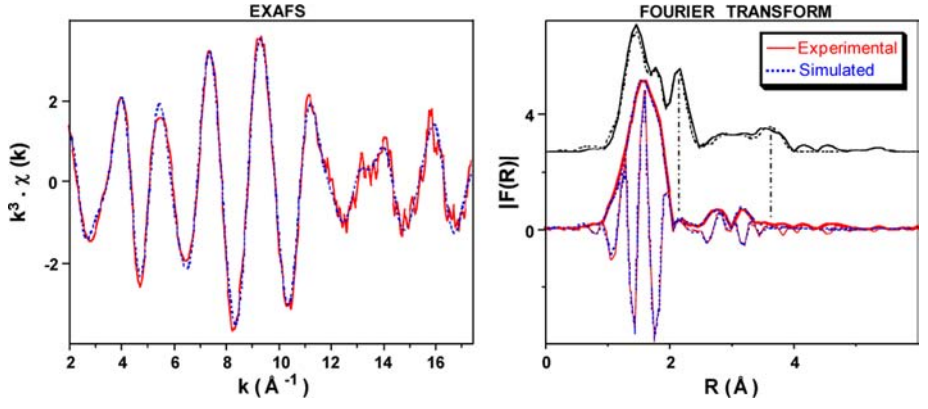

Figure 5. Tungsten L_{III}-edge k^3-weighted EXAFS (left), for the sample resulting from the grafting reaction of **3** onto SiO_{2-700} and corresponding Fourier transform (right; modulus and imaginary part; in black: Fourier transform corresponding to complex **3** for comparison), superimposed with simulated curves. Solid lines, experimental; dashed lines, spherical wave theory.

dx.doi.org/10.1021/ic401521m | Inorg. Chem. 2013, 52, 10119−10130

Table 2. EXAFS Parameters for the Supported Complex Resulting from Grafting of 3 onto SiO_{2-700}[b]

type of neighbor	no. of neighbors	distance (Å)	σ^2 (Å^2)
W=O	1	1.703(5)	0.0015(5)
W-OSi≡	1.1(5)	1.98(2)	0.0029(10)
W-CH_2CMe_3	2.9[c]	2.11(1)	0.0027(7)
W-CH_2CMe_3	2.9[c]	3.28(3)	0.0042(15)
W−OSi≡[d]	1.1[c]	3.54(4)	0.009(5)

[a]

[a]The errors generated by the EXAFS fitting program "RoundMidnight" are indicated in parentheses. [b]Δk: [2.0 − 17.4 Å^{-1}] − ΔR: [0.7−3.6 Å] ([0.7−2.3 Å], when considering only the first coordination sphere); S_0^2 = 0.94; ΔE_0 = 8.1 ± 2.0 eV (the same for all shells); fit residue: ρ = 3.3%; quality factor: $(\Delta\chi)^2/\nu$ = 1.67 (ν = 17/30) ($[(\Delta\chi)^2/\nu]_1$ = 3.22 with ν = 9/17, considering only the first coordination sphere). [c]Shell constrained to a parameter above. [d]Two (W−O−Si) types multiple scattering pathways (3 and 4 legs) have also been considered in the fit but not mentioned in this table.

2). Such reactivity is reminiscent of tungsten aqueous organometallic chemistry described by Schrock and Lippard.[12] This is also in line with previous examples demonstrating a higher selectivity toward metal−oxygen cleavage compared to that of metal−carbon,[16] though counterexamples have also been reported.[17]

Catalytic performances of the material obtained from reaction of **3** with SiO_{2-700} in propene metathesis were probed in a flow reactor (20 mL of C_3H_6 min^{-1}; 30 mol of C_3H_6 mol$_W^{-1}$ min^{-1}). A cumulated turnover numbers (TON) of 21 950 was reached after 90 h. As expected, the activity and selectivity are analogous to the values observed with the surface species **2** prepared from **1** and SiO_{2-700}. This is a further confirmation that the same precatalytic species is produced in both cases. The activity remained constant with time on stream, as previously observed.[6] From the practical point of view, this shows that the metathesis precatalyst **2** can now be accessed using **3** as the molecular precursor that is much simpler to prepare and handle than highly sensitive tetraalkyl oxo species **1**.

DFT Calculations on Models of Surface Species. Taking into account the above experimental data, we performed DFT calculations to confirm and further refine the understanding of the grafting reaction of complex **3** onto silica dehydroxylated at 700 °C (SiO_{2-700}). In the continuation of our previous theoretical studies of surface chemistry,[18] we considered as surface model the polyoligosilsesquioxane derivative **c** (Figure 6). The two upper silicon atoms, connected by a siloxane bridge, reproduce the emerged part of the silica surface, i.e., an isolated silanol group according to the infrared studies (Figure 2) for a silica dehydroxylated at 700 °C. This layer is surrounded by a layer built around four silicon atoms, themselves surrounded by another layer formed by two silicon atoms added in order to increase the rigidity of the model. For the two first layers, the silicon atoms are connected to O-SiH_3 groups, which represent the continuity of the silica surface, whereas for the last layer, both silicons are connected to hydroxyl groups in order to saturate the model.

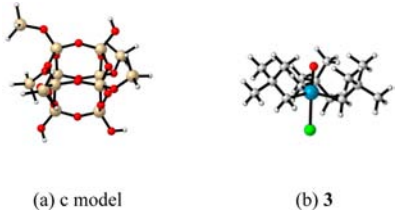

Figure 6. Representation of the optimized structures of (a) the c model of SiO_{2-700} silica surface and (b) compound **3**.

To shed light on the grafting reaction of complex **3** onto SiO_{2-700}, the W−Cl silanolysis with the concomitant HCl production as well as the W−Np silanolysis leading to the production of free CMe_4 have been considered. Other alternative pathways, such as oxo protonation by a silanol, as proposed by Herrmann and Basset for the grafting of a nitride species,[19] are found to be 18.5 kcal mol^{-1} higher in energy than our lowest energy pathway. Thus, the following discussion is reduced to the W−Cl and the W−Np silanolysis. The Gibbs-free energy profiles of both grafting reactions are depicted in Figure 7. The key geometrical parameters of the different

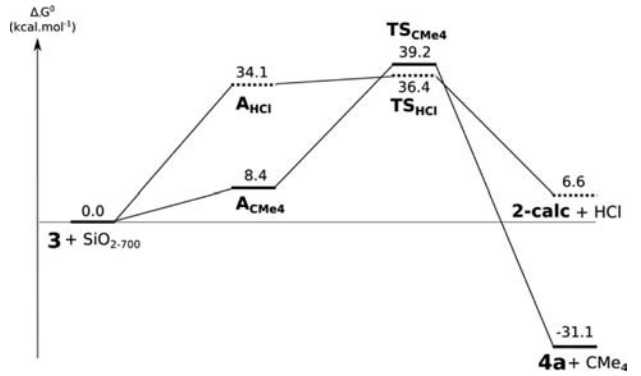

Figure 7. Energy profile for the grafting reaction of **3** onto c model.

stationary points are gathered in Table 3. The grafting reaction begins, in both cases, by the formation of an endergonic adducts $\mathbf{A_{HCl}}$ (W−Cl silanolysis, Figure 8a) and $\mathbf{A_{CMe4}}$ (W−Np silanolysis, Figure 8d), located respectively at +34.1 and +8.4 kcal mol^{-1} with respect to the entrance channel. Both adducts were obtained by an IRC calculation. This stability difference is mainly due to the interaction between **3** and **c** in both adducts. Indeed, for $\mathbf{A_{CMe4}}$, as we can see in Table 3, the structure of the [$WONp_3Cl$] moiety is almost identical to that of the free **3** complex. The endergonic formation of $\mathbf{A_{CMe4}}$ corresponds to the loss of entropy due to the formation of adduct. For $\mathbf{A_{HCl}}$, the second-order perturbation of the NBO's analysis reveals a higher donation from the long pair of the silanol oxygen atom to an empty p orbital of the metal center. This interaction can take place through an energetically costly Berry pseudorotation of **3**, from a trigonal-bipyramidal to a square-pyramidal geometry, which explains the endergonic formation of $\mathbf{A_{HCl}}$. Hoffmann et al.[20] have shown that the presence of three strong σ-donor ligands in the equatorial plane highly stabilizes a trigonal-bipyramidal geometry due to interaction of the orbitals of the ligands and the d_{xz} and d_{yz} orbitals (of e″ symmetry) of the metal center. The interaction of the orbitals of the three strong σ-donor ligands and the d_{xy} orbitals (of b_2 symmetry) of the metal center in the square-pyramidal geometry is not favorable, which explains the high cost of the Berry pseudorotation. Subsequently from $\mathbf{A_{HCl}}$, the grafting reaction takes place via transition state $\mathbf{TS_{HCl}}$ (Figure 8b). The activation energy for this reaction is calculated to be 36.4 kcal.mol^{-1} with respect to the entrance channel (+2.3 kcal

dx.doi.org/10.1021/ic401521m | Inorg. Chem. 2013, 52, 10119−10130

Table 3. Selected DFT-Calculated Bond Lengths (Å) within Molecular and Grafted Complexes

	molecular complexes		supported complexes							
	3	**3b**	$\mathbf{A_{HCl}}$	$\mathbf{TS_{HCl}}$	**2-calc**	**2b-calc**	$\mathbf{A_{CMe4}4}$	$\mathbf{TS_{CMe4}}$	**4a**	**4b**
energies	0.0	+19.0			0.0	+13.4			0.0	7.6
type of neighbor					distance (Å)					
W═O	1.703	1.687	1.674	1.679	1.713	1.692	1.703	1.698	1.703	1.686
W-OSi≡			2.669	2.332	1.993	1.910	4.921	2.310	1.863	1.883
W-CH_2CMe_3[a]	2.124	2.189	2.152	2.134	2.134	2.196	2.120	2.214	2.130	2.184
W-CH_2CMe_3[b]	3.706	3.586	3.715	3.735	3.668	3.571	3.723	3.755	3.701	3.756
W-OSi≡			4.284	3.936	3.535	3.417	5.876	3.725	3.381	3.477
W−Cl	2.460	2.321	2.675	3.253			2.470	2.428	2.461	2.356
H-O-Si≡			0.998	1.088			0.962	1.288		
Cl-H-OSi≡			1.976	1.716						
≡Si−O-H-CH_2CMe_3								1.327		

[a]Average value of the three W-CH_2CMe_3 distances; [b]Average value of the different W-CH_2CMe_3 distances (only the bond distances less than 4.0 Å were taken into account).

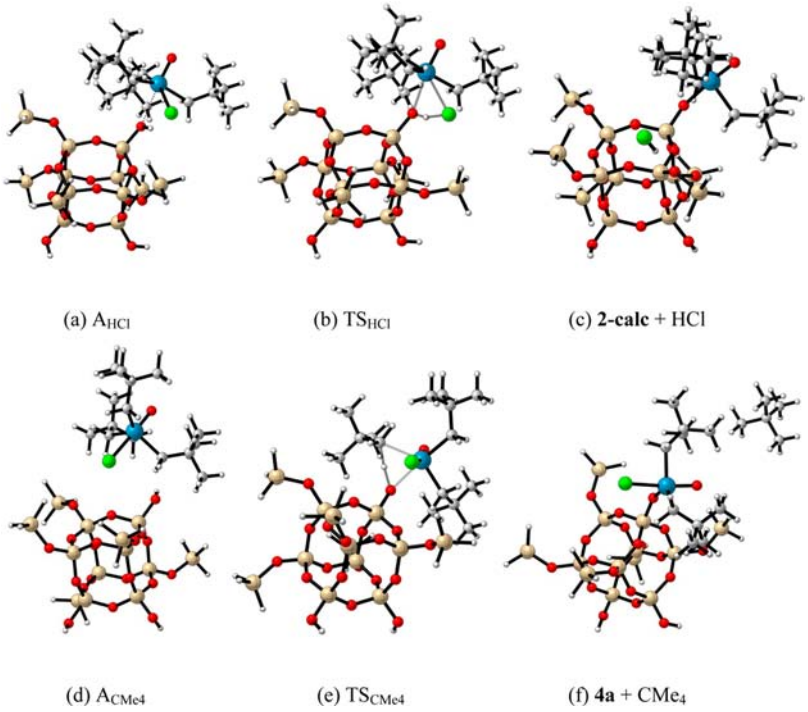

Figure 8. Optimized structures of complexes involved in the grafting reaction of **3** onto c model.

mol^{-1} with respect to $\mathbf{A_{HCl}}$). Taking into account dispersion corrections by means of using M06 functional[21] slightly reduces the barrier to 28.6 kcal mol^{-1}. From a geometrical point of view, for $\mathbf{TS_{HCl}}$, the W−O−Si≡ distance is shortened compared to $\mathbf{A_{HCl}}$ (by 0.337 Å) and the W−Cl and H-OSi≡ distances are elongated (by 0.578 and 0.090 Å, respectively). However, the two structures of $\mathbf{TS_{HCl}}$ and $\mathbf{A_{HCl}}$ remain quite similar, in good agreement with their small Gibbs free energy difference. From $\mathbf{A_{CMe4}}$, the grafting reaction takes places via transition state $\mathbf{TS_{CMe4}}$ (Figure 8e). The activation energy for this reaction is calculated to be 39.2 kcal.mol^{-1} with respect to the entrance channel (+30.8 kcal.mol^{-1} with respect to $\mathbf{A_{CMe4}}$). The M06 value of the barrier is 35.1 kcal mol^{-1}. Thus, this TS is 2.8 kcal mol^{-1} (6.6 kcal mol^{-1} using M06) higher than the formation of **2-calc**. Thus, $\mathbf{TS_{HCl}}$ is kinetically favored and **2-calc** is the kinetic product, **4a** being the thermodynamic one. For $\mathbf{TS_{CMe4}}$, as for $\mathbf{TS_{HCl}}$, an energetically costly Berry pseudorotation of **3** is necessary in order to allow the formation of an interaction between the metal center and the silanol group. As we can see in Figure 9, the alternation of the natural charges between the atoms in $\mathbf{TS_{HCl}}$ are slightly more favorable than on $\mathbf{TS_{CMe4}}$ leading to a slightly smaller activation barrier. This is in line with the difference of trans effect (O vs Cl) in

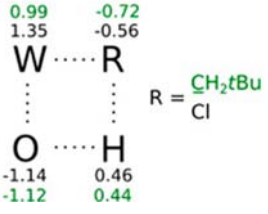

Figure 9. Natural charges of the atoms involved in the sylanolysis reaction in TS_{HCl} and TS_{CMe4}.

dx.doi.org/10.1021/ic401521m | Inorg. Chem. 2013, 52, 10119−10130

Scheme 4. Synthesis of ^{17}O-Labeled Species

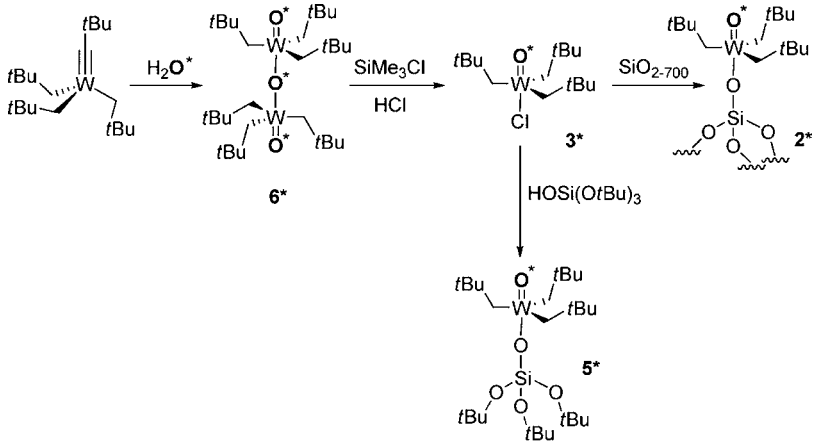

each TS but the greater steric hindrance in $\mathbf{TS_{CMe4}}$ than in $\mathbf{TS_{HCl}}$ also accounts for the difference of stability.

The formation, through $\mathbf{TS_{CMe4}}$, of **4a** with concomitant CMe_4 production (Figure 8f) is exoergonic by −31.1 kcal.mol^{-1} with respect to the starting material. In **4a**, the tungsten atom adopts a distorted trigonal bipyramidal geometry with two neopentyl ligands and the oxygen atom of the silica surface in equatorial sites; the oxo and chloride ligands occupying the two axial sites. The square pyramidal isomer **4b** (see Figure S7 in the Supporting Information) is less stable by 7.6 kcal.mol^{-1}. The formation of **2-calc** with concomitant HCl production (Figure 8c), from $\mathbf{TS_{HCl}}$, is calculated to be slightly endergonic by 6.6 kcal.mol^{-1} with respect to the separated reactants. The released HCl could then further react with the reaction medium leading to a global athermic process, which is consistent with a reversible reaction, as experimentally observed. In **2-calc**, the tungsten atom adopts a slightly distorted trigonal bipyramidal geometry with the three neopentyl ligands in equatorial sites; the oxo and the oxygen atom of the silica surface occupying the two axial sites. The square pyramidal isomer **2b-calc** (see Figure S7 in the Supporting Information) is less stable by 13.4 kcal.mol^{-1}. In both cases, according to the energy difference between the trigonal bipyramidal isomer and the square planar one, we can safely conclude that only one conformation can exist.

Experimental and Theoretical Approaches to ^{17}O NMR. The ^{17}O NMR chemical shift has been tentatively used as a probe for molecular vanadium-oxo organometallic systems in liquid state NMR.[22] However, authors noticed that the rather narrow chemical shift range did not allow drawing a correlation between CS and the metal coordination sphere. This emphasizes that one cannot efficiently rely on this descriptor alone to draw conclusions about the structure of organometallic oxo species. On the other hand, solid-state NMR data should afford a further layer of information, from quadrupolar and chemical shift interactions. Under MAS conditions, a close analysis of (i) the shape of individual spinning sideband and (ii) the total spectral pattern provides a large set of anisotropic parameters (C_Q, η_Q, Δ_{CSA}, and η_{CSA}), in addition to the isotropic chemical shift to well characterize the oxygen environment. When coupled to DFT calculation, this may prove to be very successful as a method for the determination of the nature of the related species. As highly characteristic spectroscopic features are expected, calculation of the expected values for a postulated structure should be confronted to experimental data and thus confirm or invalidate a proposed structure.

To generate a set of data amenable to trends assessment, we compared several ^{17}O-enriched molecular oxo species (**3***, **5***, and **6***, that latter featuring both terminal and bridging oxo ligands), along with hybrid material **2***. The labeling scheme to access to surface species [(≡SiO)WO*Np_3] (**2***) is described in Scheme 4. The first step consists in the hydrolysis of [W(≡C*t*Bu)Np_3] using 70%-^{17}O-enriched water to afford the trisoxo alkyl dinuclear complex [O($WONp_3$)$_2$] **6***, where both the bridging and terminal positions are labeled.[12] From this complex, the chloride derivative **3*** is obtained through treatment with $SiMe_3Cl$/HCl, and its reaction with SiO_{2-700} and HOSi(O*t*Bu)$_3$ provides **2*** and its ^{17}O-tagged molecular model, **5***, respectively.

Isotopic labeling is evidenced in the case of **5*** by a shift in the position of the W=O band, from 1006 to 998 cm^{-1}. The higher position compared to that of the expected theoretical one (977 cm^{-1}) is most probably due to the fact that it consists of a combination of vibrations and not of pure $\nu_{(W=O)}$. Indeed, the IR spectrum computed at the DFT level displays a band at 1012 cm^{-1}that corresponds to a coupled vibration involving elongation of the terminal oxo $\nu_{(W=O)}$ and elongation of the (Si)O−W $\nu_{(W-O(Si))}$.

With this series of species at hand, we recorded the ^{17}O MAS NMR spectrum of molecular species **3***, **5***, and **6*** (Figure 10). At first, one should mention that the presence of large CSA and quadrupolar couplings afford spectra featuring numerous spinning sidebands, each one characterized by specific line shape and amplitude. The mononuclear complexes **3*** and **5*** give rise to similar spectra, regarding both the discontinuities of resonance at the isotropic chemical shift, and the spinning sidebands pattern. Their chemical shift are very close (735 and 731 ppm for **3*** and **5***, respectively, Table 4). These values are in line with reported values for other tungsten oxo species featuring W=O and W−O−W moieties.[23] However, as previously mentioned, the similarity between the observed values means that the chemical shift alone is not an appropriate parameter to assess structural changes when comparing the influence of the presence a chloride and an alkoxide ligand in the position trans to the oxo moiety. The quadrupolar coupling constant deduced at first sight from the width of the signal at δ_{CS} is larger for **5***, which shows that other parameters may prove more appropriate than chemical shift as descriptors. These are related to anisotropy of chemical

dx.doi.org/10.1021/ic401521m | *Inorg. Chem.* 2013, 52, 10119−10130

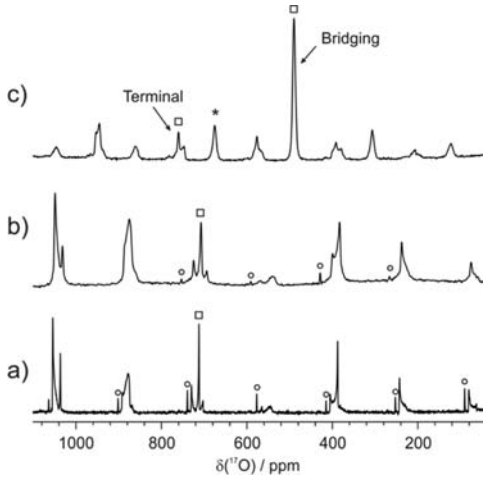

Figure 10. ^{17}O MAS NMR spectra of (a) **3*** (18.8 T, number of scans ns =2048, recycling delay rd =5 s, MAS rate =17.6 kHz); (b) **5*** (18.8 T, ns =32768, rd =1 s, MAS rate =17.6 kHz); and (c) **6*** (18.8 T, ns =15000, rd =5 s, MAS rate =20 kHz); For the sake of clarity, the signals at isotropic chemical shift are marked with □; ○, impurity.

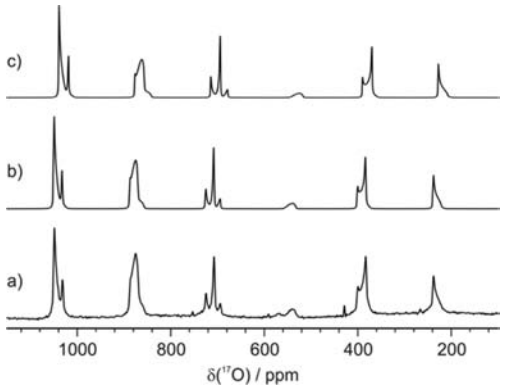

Figure 11. ^{17}O MAS NMR spectra of **5***: (a) experimental, (b) SIMPSON best fit simulation, and (c) calculated from DFT parameters.

shift and quadrupolar coupling. As mentioned above, they are available through the description of the whole spectral pattern. To determine such parameters, we relied on simulations with the SIMPSON program.[24] Indeed, as the spectra present highly characteristic discontinuities, along with specific features for each sideband, it is possible to determine them with good accuracy (see below). Earlier ^{17}O cases have been reported on samples under static conditions retaining both quadrupolar and CSA specific features at the expense of the sensitivity.[25] On the other hand, under spinning sample conditions, these spectroscopic features can be analyzed from the experimental data on systems with moderate quadrupolar coupling.[26] Here the large magnitude of both quadrupolar and CSA interactions at high magnetic field allows for a complete analysis of the MAS spectrum. From optimization of simulations, it is possible to assess the influence of each anisotropic parameter on the spectrum: A systematic approach has been followed, as described in the Supporting Information (Figure S2). Consecutive optimization of the various parameters allows for converging toward a single set of parameters. In summary, the quadrupolar parameters (C_Q, η_Q) mostly affect the shape of each spinning sideband, whereas the CSA parameters (Δ_{CSA} and η_{CSA}) are responsible for the total envelop of the spectrum, i.e., the relative intensity of the spinning sidebands. Results are presented in Table 4, and the best fit for **5*** is presented in Figure 11 (see the Supporting Information for similar data related to **3***). The precision of the parameters determination in the case of archetypical **5*** has been assessed to below ±3 and 75 ppm for CS and Δ_{CSA}, respectively, 0.2 MHz for C_Q, and 0.1 for both η_Q and η_{CSA} (see Figures S4−S8 in the Supporting Information).

DFT calculated values are in very good agreement for most of the anisotropic parameters. The line shape of the resonance at δ_{CS} = 731 ppm is very well reproduced, along with the relative intensities and line shapes of spinning side-bands (see the Supporting Information for corresponding data for **3*** and **6***). The Euler angles (α, β, γ) describing the relative orientation of the quadrupolar and CSA tensors also affect the line shape. Here, the β angle has been assessed to 0°, which indicates that CSA and quadrupolar tensors are collinear (see Supporting Information).

Dimer **6*** presents two sets of signals accounting for the bridging and terminal oxo moieties (Figure 10c and Table 4). The terminal W═O site gives rise to a resonance at the isotropic chemical shift with a line shape that is comparable to that of **3*** and **5***, at higher chemical shift (775 ppm compared to 735 and 731 ppm for **3*** and **5***, respectively). The bridging oxygen features are strongly different in terms of isotropic chemical shift (490 ppm, in good agreement with literature data on W−O−W systems[23]) and quadrupolar coupling constant (1.0 MHz). Compared to the mononuclear species **3*** and **5***, larger errors on calculated chemical shift values for **6*** are obtained (17% and 7% for bridging and terminal oxo moieties, respectively), which is acceptable considering the large ^{17}O chemical shift range. Regarding the DFT optimized structure of **6**, if we consider the two terminal oxo moieties, for which the relative error compared to the experiment is the worst, one can

Table 4. Experimental and DFT-Calculated ^{17}O NMR Parameters for Species 2−6

	CS (ppm)		C_Q (MHz)		η_Q		Δ_{CSA}		η_{CSA}	
species	expt	calcd	expt	calcd	expt	calcd	expt	calcd	expt	calcd
2[b]	757	758	5.3	5.7	0.20	0.17	−1200	−1136	0.15	0.07
3	735	701	5.1	5.2	0.01	0.11	−1110	−1109	0.07	0.07
4a		730		4.6		0.55		−945		0.77
4b		757		2.2		1.0		−948		0.42
5	731	721	5.44	5.8	0.09	0.02	−1125	−1128	0.05	0.05
6: O_{term}	775	718[a]	4.6	6.0[a]	0.9	0.00[a]	−900	−1112[a]	0.85	0.00[a]
O_{bridge}	490	405	1.0	0.9	0.01	0.03	−405	−350	0.8	0.02

[a]Averaged value between the two terminal oxo moieties. [b]Calculated values have been obtained with the **2-calc** structure.

dx.doi.org/10.1021/ic401521m | Inorg. Chem. 2013, 52, 10119−10130

observe different C−H···O interactions (see Figure 12). These interactions are probably responsible for the difference between

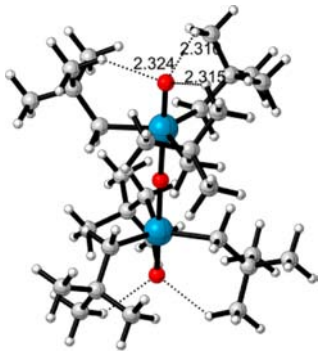

Figure 12. C−H···O interactions in DFT-optimized **6**.

experimental and theoretical values. As a matter of fact, if dynamics effects were considered, these interactions would virtually disappear, leading to a signal closer to the experimental value.

Thus, the satisfying adequacy between experimental and theoretical ^{17}O NMR validates our combined approach, a most critical prerequisite for structural determination for compounds or sites of unknown nature.

Hybrid material **2*** features a ^{17}O NMR spectrum that is characteristic of high quadrupolar and chemical shift anisotropy (Figure 13). The isotropic chemical shift is in the expected region (757 ppm). One notices that global signal envelope (relative intensities of spinning sidebands) is similar to that of above-described molecular oxo compounds, most particularly regarding the terminal W═O moiety. Within the limits of detection, this set of bands is consistent with the presence of a single type of W−O in material **2***, in agreement with the other

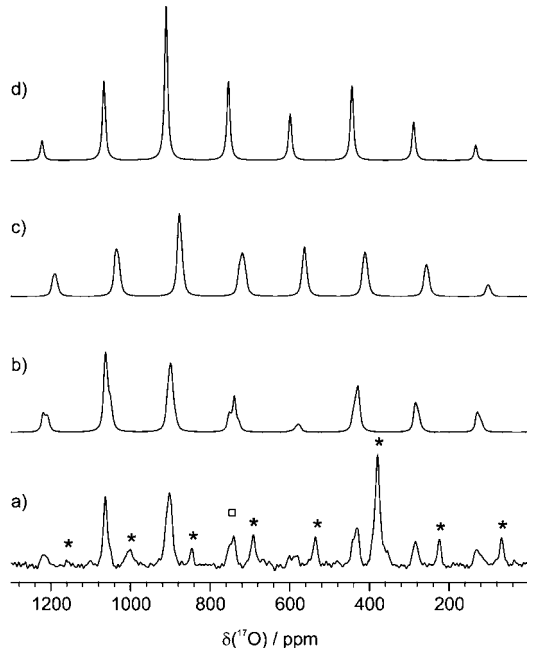

Figure 13. ^{17}O MAS NMR spectrum of **2*** (21.15 T, ns = 59756, rd = 1s, MAS rate = 19 kHz), and DFT-calculated ^{17}O MAS NMR spectrum of (b) **2***, (c) **4a**, and (d) **4b**. Asterisks designate the rotor's ZrO_2 signal. The signal at isotropic chemical shift is marked with □.

experimental techniques used above. The signal at isotropic chemical shift presents a noticeable discontinuity which indicates significant quadrupolar coupling constant. The spinning sidebands show a much lesser degree of discontinuity, stemming from the distribution in the local structure of the surface organometallic sites. Indeed, even if the first coordination sphere remains the same (namely, [(≡SiO)-$WONp_3$]), as the surface is amorphous, medium range interactions affect the ^{17}O signal. We have already observed in related systems that ^{17}O NMR signal is very sensitive to local structure.[10] To assess the structure of the tungsten oxo species and settle between W−C and W−Cl cleavage pathways upon grafting of **3**, we compared the theoretical spectra resulting from DFT-calculated structures **2-calc**, **4a**, and **4b** using the SIMPSON program (Figure 13b−d, respectively) to that of **2*** (Figure 13a). A line broadening of 1000 Hz was applied to account for the local structural distribution mentioned above. As mentioned above, chemical shift alone cannot give a clear-cut answer, as DFT accuracy level is too low compared to the actual experimental range. However, anisotropy is expected to provide unambiguous information, as it governs the whole spectral line shape, both in individual bands and in the overall envelope. When comparing calculated spectra for **2-calc** (DFT optimized model for the grafting of **3** via W−Cl cleavage), **4a** and **4b** (DFT optimized isomeric models for the grafting of **3** via W−C cleavage), only that of **2-calc** reproduces key features of the experimental data: the discontinuity of the δ_{CS} signal, and the low intensity of the first spinning sideband at higher field. Indeed, both **4a** and **4b** feature significantly lower calculated Δ_{CSA} and C_Q values compared to data of **2-calc** (Table 4). This not only confirms that the DFT approach is efficient in this case, but is also fully in line with the above-described characterization of **2** that demonstrated the reaction via W−Cl and not by W−C cleavage.

■ CONCLUSION

The grafting chemistry of the oxo organometallic tungsten derivative [$WOClNp_3$] onto silica dehydroxylated at 700 °C was explored. Reactivity proceeds via cleavage of a W−Cl bond, and not by W−C silanolysis, affording well-defined surface species [(≡SiO)$WONp_3$] under optimized reaction conditions. This was demonstrated by a set of complementary analytical and spectroscopic techniques. DFT calculations also allowed rationalizing both the grafting pathway and the experimentally observed reversibility of this reaction under static conditions. This hybrid material is an efficient precatalyst for propene metathesis, featuring high activity and stability. Efficient ^{17}O-labeling scheme of the oxo moiety was performed for a series of molecular and supported oxo organometallic tungsten derivatives. Indeed, ^{17}O NMR provided a large set of parameters, including quadrupolar coupling and chemical shift which are best suited to describe local structure of an oxygen atom. Combined to DFT calculations on molecular and more challenging surface species, this approach efficiently confirmed the observed W−Cl cleavage process, and ruled out other grafting pathways, thanks to highly characteristic spectral features. This study will pave the way toward future development of supported organometallics that model the postulated active sites of industrially relevant catalysts, such [$(O_s)_2WO(═CHR)$].[27] One of the most attractive entries into this chemistry will be use of mildly dehydroxylated silica support, which is known to have a less straightforward surface chemistry.[9] In such a context, use of ^{17}O MAS NMR combined

dx.doi.org/10.1021/ic401521m | Inorg. Chem. 2013, 52, 10119−10130

to DFT calculations will definitively be a strong point to successfully meet this challenge.

EXPERIMENTAL SECTION

All experiments were carried out by using standard Schlenk and glovebox techniques. Solvents were purified and dried according to standard procedures. C_6D_6 (SDS) was distilled over Na/benzophenone and stored over 3 Å molecular sieves. Complexes **3**[7a] and [W(≡C*t*Bu)Np_3][28] were synthesized following the literature procedure. ^{17}O-enriched **3*** and **6*** were prepared using the reported procedure using ^{17}O labeled water.[12b] Propene was dried and deoxygenated before use by passing it through a mixture of freshly regenerated molecular sieves (3 A) and $R\bar{3}$−15 catalysts (BASF). SiO_{2-700} was prepared from Aerosil silica from Degussa (specific area of 200 $m^2\ g^{-1}$), which was partly dehydroxylated at 700 °C under high vacuum (10^{-5} Torr) for 15 h to give a white solid having a specific surface area of 190 $m^2\ g^{-1}$ and containing 0.7 OH nm^{-2}. Gas-phase analyses were performed on a Hewlett-Packard 5890 series II gas chromatograph equipped with a flame ionization detector and an Al_2O_3/KCl on fused silica column (50 m X 0.32 mm). Elemental analyses were performed at the Pascher Mikroanalytisches Labor at Remagen-Bandorf (Germany). IR spectra were recorded on a Nicolet 6700 FT-IR spectrometer by using a DRIFT cell equipped with CaF_2 windows. The samples were prepared under argon within a glovebox. Typically, 64 scans were accumulated for each spectrum (resolution 4 cm^{-1}). Confocal Raman spectra were acquired using the 488 nm line of a Ar-ion laser (Melles Griot). The excitation beam was focused on the sample by a 50× long working distance microscope and the scattered light was analyzed by an air-cooled CCD (Labram HR, Horiba Jobin Yvon). The fluorescence was subtracted from the spectra for clarity.

NMR Characterization. Solution NMR spectra were recorded on an Avance-300 Bruker spectrometer. All chemical shifts were measured relative to residual ^{1}H or ^{13}C resonances in the deuterated solvent: C_6D_6, δ 7.15 ppm for ^{1}H, 128 ppm for ^{13}C. ^{1}H and ^{13}C solid-state NMR spectra were recorded on Bruker Avance-500 spectrometers with a conventional double-resonance 4 mm CP-MAS probe at the Laboratoire de Chimie Organométallique de Surface. In all experiments, the rotation frequency was set to 10 kHz unless otherwise specified. Chemical shifts were given with respect to TMS as external reference for ^{1}H and ^{13}C NMR. The ^{17}O solid-state NMR spectra were acquired on Bruker Avance III 800 (^{1}H, 800.13 MHz, ^{17}O, 108.47 MHz) and 900 (^{17}O, 122.11 MHz) spectrometers. For ^{1}H experiments, the spinning frequency was 20 kHz, the recycle delay was 5 s, and 16 scans were collected using a 90° pulse excitation of 2.25 μs. The ^{17}O MAS NMR spectra at 18.8 and 21.15 T were acquired at spinning frequencies ranging from 17.6 to 20 kHz (3.2 mm rotor diameter) to avoid overlapping of spinning sidebands with CS resonances.

Preparation and Characterization of [{(tBuO)$_3$SiO}WONp$_3$] (5). 3. (100 mg, 0.22 mmol) and HOSi(O*t*Bu)$_3$ (59 mg, 0.22 mmol) were stirred in 30 cm^3 of pentane for 5 h at room temperature with a constant bubbling of argon to remove the HCl released. The solvent was then removed under vacuum to leave a white solid. The crude material was crystallized from pentane at −30 °C to yield 0.125 g of complex **5** (85% isolated yield). δ(^{1}H, C_6D_6): 2.19 (6 H, s, $CH_2C(CH_3)_3$, $^2J_{(WH)}$= 12.0 Hz), 1.43 (24 H, s, $OC(CH_3)_3$), 1.35 (24 H, s, $CH_2C(CH_3)_3$). δ(^{13}C{^{1}H}) (C_6D_6): 92.3 [$CH_2C(CH_3)_3$, $^1J_{(WC)}$= 93.4 Hz), 72.5 (s, $OC(CH_3)_3$), 35.4 (s, $CH_2C(CH_3)_3$), 33.0 (s, $OC(CH_3)_3$), 31.9 (s, $CH_2C(CH_3)_3$). IR: 1006 cm^{-1} ($\nu_{W=O}$) Anal. Calcd for $C_{27}H_{60}O_5SiW$: C, 47.92; H, 8.94%. Found: C, 48.04; H, 9.02%.

Preparation and Characterization of 3/SiO_{2-700}. A mixture of finely ground **3** (150 mg, 0.33 mmol) and SiO_{2-700} (1 g) were stirred at 25 °C under dynamic vacuum for 4 h, whereas all volatile compounds were condensed into a cold trap. Pentane was then added and the solid was washed 5 times. The resulting white powder was dried under vacuum (1 × 10^{-5} Torr). Analysis by infrared spectroscopy of the condensed volatiles indicated the formation of 223 μmol of HCl during the grafting (0.9 HCl/W). Elemental anal.: W 4.02 wt %; C 4.02 wt %; H 0.69 wt %. ^{1}H MAS NMR (800 MHz) δ 2.1, 1.1 ppm. ^{13}C CP MAS NMR (200 MHz) δ 92, 35, and 31 ppm.

Procedure for the Quantification of HCl Released during Grafting. The gas phase released during grafting was condensed into an IR-cell equipped with CaF_2 windows. Transmission infrared spectra were recorded on a Nicolet Magna 5700 FT spectrometer, at room temperature. The resolution was 1 cm^{-1} with 16 scans. HCl was quantified by comparison of the surface of the absorbance IR bands in the 2600−3100 cm^{-1} region of the sample to a calibration curve. For the calibration, known amounts of pure HCl were introduced into the same gas cell and identical parameters (resolution, number of scans, integration width, and baseline) were used.

SIMPSON Simulation of ^{17}O MAS NMR Spectra. All ^{17}O MAS NMR numerical spectra were calculated using *gcompute* method implemented in SIMPSON software package[24] to reproduce chemical shift anisotropy and quadrupolar interaction effects observed on experimental data. This package described each line shape with nine NMR interaction parameters, which included the isotropic chemical shift (δ_{CS}) defined in eq 1, the quadrupole coupling constant (C_Q) and quadrupole asymmetry parameter (η_Q) defined in eqs 2 and 3, the CSA (Δ_{CSA}) and chemical shift asymmetry parameter (η_{CSA}) (in the Haeberlen convention) defined in eqs 4 and 5, and the Euler angles (α, β, γ). Each numerical simulation was performed with the zcw4180 crystallite file and 20 gamma angles, with the calculated FID inclusive of all quadrupolar satellites. To better fit experimental and calculated spectra, we applied a Gaussian line broadening of 120 and 1000 Hz for ^{17}O MAS spectra of molecular and grafted compounds, respectively.

$$\delta_{CS} = (\delta_{11} + \delta_{22} + \delta_{33})/3 \quad (1)$$

$$C_Q = e^2qQ/h = eV_{33}Q/h,\ |V_{33}| \geq |V_{22}| \geq |V_{11}| \quad (2)$$

$$\eta_Q = (V_{11} - V_{22})/V_{33},\ (1 \geq \eta_Q \geq 0) \quad (3)$$

$$\Delta_{CSA} = \delta_{zz} - (\delta_{xx} + \delta_{yy})/2 = 3\delta/2,\ |\delta_{zz} - \delta_{CS}| \geq |\delta_{xx} - \delta_{CS}| \geq |\delta_{yy} - \delta_{CS}| \quad (4)$$

with the reduced anisotropy, $\delta = \delta_{33}$-δ_{CS}

$$\eta_{CSA} = (\delta_{yy} - \delta_{xx})/(\delta_{zz} - \delta_{CS}),\ (1 \geq \eta_{CSA} \geq 0) \quad (5)$$

DFT Methodological Details. All DFT calculations were performed with Gaussian 03.[29] Calculations were carried out at the DFT level of theory using the hybrid functional B3PW91.[30] Geometry optimizations were achieved without any symmetry restriction. Calculations of vibrational frequencies were systematically done in order to characterize the nature of stationary points. Stuttgart effective core potentials and their associated basis set were used for silicon and tungsten.[31] The basis sets were augmented by a set of polarization functions (ζd = 0.284 for Si and ζf = 0.823 for W). Hydrogen, carbon, chlorine, and oxygen atoms were treated with 6-31G(d,p) double-ζ basis sets.[32] The optimized structures were used for ^{17}O NMR calculations. These calculations were also performed using a higher Duninng's correlation consistent basis set cc-PVTZ for the oxygen atoms.[33] In all cases, among the various theories available to compute chemical shielding tensors, the Gauge Including Atomic Orbital (GIAO) method has been adopted for the numerous advantages it presents.[34] Typically, in order to compare our calculations with experimental values, ^{17}O chemical shielding has been converted to chemical shift using the usual equation: $\delta_{iso} = \sigma_{iso\ ref} - \sigma_{iso\ sample}$, where $\sigma_{iso\ ref}$ is the isotropic ^{17}O chemical shielding of the liquid water. However, because of the arbitrariness in the choice of the isotropic chemical shift of the reference - the value of $\sigma_{iso\ ref}$ depends on the level of theory and the used basis sets[35]- an internal reference is used for the calibration of the $\sigma_{iso\ ref}$ value. As a consequence, we have calibrated the $\sigma_{iso\ ref}$ value with respect to the ^{17}O CS of isolated silanol groups without interaction with organometallic fragments, i.e., the calculated $\sigma_{iso\ sample}$ of 287.6 ppm is attributed to an experimental CS of 4.6 ppm: $\sigma_{iso\ ref}$ = 292.2 ppm. The ^{17}O quadrupolar coupling constant C_Q and the asymmetry parameter η_Q, which describes the

dx.doi.org/10.1021/ic401521m | *Inorg. Chem.* 2013, 52, 10119−10130

interaction between nuclear quadrupolar moment of the oxygen nuclei with the electric field gradient (EFG) arisen at these sites, are calculated from the EFG tensor eigenvalues V_{11}, V_{22}, and V_{33} following eqs 2 and 3.

EXAFS. X-ray absorption spectra were acquired at the SRS of the CCLRC in Daresbury (UK), using beamline 9.3 (project 50049), at room temperature at the tungsten L_{III} edge, with a double crystal Si(111) monochromator detuned 70% to reduce the higher harmonics of the beam. The spectra were recorded in the transmission mode between 10.05 and 11.45 keV. The supported W sample was packaged within a nitrogen filled drybox in a double airtight sample holder equipped with kapton windows. This type of cell has already been used and proved to be very efficient for air-sensitive compounds such as ≡SiO-HfNp$_3$ species supported onto Aerosil silica$_{(800)}$ where the Hf−C contribution could be clearly distinguished from Hf−O by EXAFS.[36] The spectra analyzed were the results of four such acquisitions and no evolution could be observed between the first and last acquisition. The data analyses were performed by standard procedures using in particular the program "Athena"[37] and the EXAFS fitting program "RoundMidnight",[38] from the "MAX" package, using spherical waves. The program FEFF8 was used to calculate theoretical files for phases and amplitudes based on model clusters of atoms.[39] The value of the scale factor, $S_0^2 = 0.94$, was determined from the k^1, k^2, and $k^3\chi(k)$ spectra of a reference compound, a sample of [W(≡C*t*Bu)Np$_3$] molecular complex diluted in BN and carefully mixed and pressed as a pellet (one carbon at 1.76(1) Å and three carbon atoms at 2.10(1) Å in the first coordination sphere, with one carbon atom at 3.25(3) Å and three carbon atoms at 3.34(3) Å). The refinements were performed by fitting the structural parameters N_i, R_i, σ_i and the energy shift, ΔE_0 (the same for all shells). The fit residue, ρ(%), was calculated by the following formula

$$\rho = \frac{\sum_k [k^3\chi_{exp}(k) - k^3\chi_{cal}(k)]^2}{\sum_k [k^3\chi_{exp}(k)]^2} 100$$

As recommended by the Standards and Criteria Committee of the International XAFS Society,[40] the quality factor, $(\Delta\chi)^2/\nu$, where ν is the number of degrees of freedom in the signal, was calculated and its minimization considered in order to control the number of variable parameters in the fits. The fits were conducted by first considering the coordinated ligands of the complexes and then by adding further backscatterers in order to improve the fits. For the molecular complex **3**, considering only the first sphere, the coordination numbers of the ligands were let free to vary and a satisfactory fit was obtained with values in agreement with the foreseen coordination numbers, within the error margins: 1.0 ± 0.1 for N_{oxo} (th. 1), 0.9 ± 0.2 for N_{Cl} (th. 1) and 3.2 ± 0.4 for N_C (th. 3). This was in particular a good validation of the theoretical phase and amplitude files used for the fit. Further improvements of the fit were carried out with integer values for neighbor numbers, known for complex **3**. In the first coordination sphere of the supported complex resulting from the reaction of **3** onto silica, once the presence of chlorine ruled out, one oxo ligand was considered and the coordination numbers of the siloxy (N_O) and neopentyl ligands (N_C) were free to vary with one constraint ($N_O + N_C = 4.0$ for W(VI)), in order to reduce the number of variable parameters in the fit but also to consider for instance the possibility of bis-siloxy tungsten complexes grafted onto silica.

■ ASSOCIATED CONTENT

Ⓢ Supporting Information

Additional experimental and simulated ^{17}O MAS NMR data, CSA and EFG tensors orientation on grafted species, and DFT optimized structures. This material is available free of charge via the Internet at http://pubs.acs.org.

■ AUTHOR INFORMATION

Corresponding Author

*E-mail: mostafa.taoufik@univ-lyon1.fr (M.T.); regis.gauvin@ensc-lille.fr (R.M.G.); laurent.delevoye@ensc-lille.fr (L.D.); laurent.maron@irsamc.ups-tlse.fr (L.M.).

Notes

The authors declare no competing financial interest.

■ ACKNOWLEDGMENTS

We thank the CNRS, UOP, the French Ministry of Research and Higher Education, and the Agence Nationale de la Recherche (ANR-12-BS07-0021-01, OXOCAT) for their generous support, and the UCCS Directing Board for an internal grant. Financial support from the TGE RMN THC Fr3050 for conducting the research is gratefully acknowledged. Laurent Maron is member of the Institut Universitaire de France (IUF). CALMIP is also acknowledged for a generous grant of computing time. We also thank Steven Fiddy, former scientist at the SRS of the CCLRC, in Daresbury, U.K., for his help during the recording of the EXAFS data at SRS beamline 9.3 (project AP 50049).

■ REFERENCES

(1) (a) Mol, J. C. *J. Mol. Catal. A* **2004**, *213*, 39. (b) Dwyer, C. L. Metathesis of Olefins. In *Metal-Catalysis in Industrial Organic Processes*; Chiusoli, G. P., Maitlis, P. M., Eds.; Royal Society of Chemistry: Cambridge, U.K., 2006.

(2) (a) Heckelsberg, L. F.; Banks, R. L.; Bailey, G. C. *Ind. Eng. Chem. Prod. Res. Dev.* **1968**, *7*, 29. (b) van Schalkwyk, C.; Spamer, A.; Moodley, D. J.; Dube, T. *Appl. Catal., A* **2003**, *255*, 121. (c) Spamer, A.; Dube, T. I.; Moodley, D. J.; van Schalkwyk, C.; Botha, J. M. *Appl. Catal., A* **2003**, *255*, 133. (d) van Schalkwyk, C.; Spamer, A.; Moodley, D. J.; Dube, T. *Appl. Catal., A* **2003**, *255*, 143.

(3) (a) Hérisson, J. L.; Chauvin, Y. *Makromol. Chem.* **1978**, *179*, 1285. (b) Chauvin, Y. *Angew. Chem., Int. Ed.* **2006**, *45*, 3740. (c) Schrock, R. R. *Chem. Rev.* **2002**, *102*, 145.

(4) Spamer, A.; Dube, T. I.; Moodley, D. J.; van Schalkwyk, C.; Botha, J. M. *Appl. Catal., A* **2003**, *255*, 153.

(5) (a) Kapteijn, F.; Bredt, H. L. G.; Homburg, E.; Mol, J. C. *Ind. Eng. Chem. Prod. Res. Dev.* **1981**, *20*, 457. (b) Handzlik, J.; Ogonowski, J. *Catal. Lett.* **2003**, *88*, 119.

(6) Mazoyer, E.; Merle, N.; De Mallmann, A.; Basset, J.-M.; Berrier, E.; Delevoye, L.; Paul, J.-F.; Nicholas, C. P.; Gauvin, R. M.; Taoufik., M. *Chem. Commun.* **2010**, *46*, 8944.

(7) (a) Kress, J.; Russel, M. J. M.; Wesolek, M.; Osborn, J. A. *J. Chem. Soc., Chem. Commun.* **1980**, 431. (b) Kress, J.; Wesolek, M.; Le Ny, J.-P.; Osborn, J. A. *J. Chem. Soc., Chem. Commun.* **1981**, 1039.

(8) Rhers, B.; Salameh, A.; Baudouin, A.; Quadrelli, E. A.; Taoufik, M.; Copéret, C.; Lefebvre, F.; Basset, J.-M.; Solans-Monfort, X.; Eisenstein, O.; Lukens, W. W.; Lopez, L. P. H.; Sinha, A.; Schrock, R. R. *Organometallics* **2006**, *25*, 3554.

(9) *Modern Surface Organometallic Chemistry*; Basset, J.-M., Psaro, R., Roberto, D., Ugo, R., Eds.; Wiley-VCH: Weinheim, Germany, 2009.

(10) Merle, N.; Trébosc, J.; Baudouin, A.; Del Rosal, I.; Maron, L.; Szeto, K.; Genelot, M.; Mortreux, A.; Taoufik, M.; Delevoye, L.; Gauvin., R. M. *J. Am. Chem. Soc.* **2012**, *134*, 9263.

(11) (a) Fischbach, A.; Klimpel, M. G.; Widenmeyer, M.; Herdtweck, E.; Scherer, W.; Anwander, R. *Angew. Chem. Int., Ed.* **2004**, *43*, 2234. (b) Gauvin, R. M.; Buch, F.; Delevoye, L.; Harder, S. *Chem.—Eur. J.* **2009**, *15*, 4382.

(12) (a) Feinstein-Jaffe, I.; Pedersen, S. F.; Schrock, R. R. *J. Am. Chem. Soc.* **1983**, *105*, 7176. (b) Feinstein-Jaffe, I.; Gibson, D.; Lippard, S. J.; Schrock, R. R.; Spool, A. *J. Am. Chem. Soc.* **1984**, *106*, 6305.

(13) Sergienko, V. S.; Kovalenko, Yu. V.; Llyukhin, A. B.; Abramenko, V. L. *Zh. Neorg. Khim.* **1994**, *0*, 1320.

(14) Clough, C. R. PhD thesis, Massachusetts Institute of Technology, Cambridge, MA, 2011, p 136.
(15) Lehtonen, A.; Sillanpää, R. *Acta Crystallogr., Sect. C* **1998**, *54*, 935.
(16) (a) Miller, J. B.; Schwartz, J.; Bernasek, S. L. *J. Am. Chem. Soc.* **1993**, *115*, 8239. (b) Meyer, T. Y.; Woerpel, K. A.; Novak, B. M.; Bergman, R. G. *J. Am. Chem. Soc.* **1994**, *116*, 10290.
(17) Chen, Y.; Callens, E.; Abou-Hamad, E.; Merle, N.; White, A. J. P.; Taoufik, M.; Copéret, C.; Le Roux, E.; Basset, J.-M. *Angew. Chem., Int. Ed.* **2012**, *51*, 11886.
(18) (a) Del Rosal, I.; Gerber, I. C.; Poteau, R.; Maron, L. *J. Phys. Chem. A.* **2010**, *114*, 6322. (b) Del Rosal, I.; Poteau, R.; Maron, L. *Dalton Trans.* **2011**, *40*, 11211. (c) Del Rosal, I.; Poteau, R.; Maron, L. *Dalton Trans.* **2011**, *40*, 11218. (d) Del Rosal, I.; Tschan, M. J.-L.; Gauvin, R. M.; Maron, L.; Thomas, C. M. *Polym. Chem.* **2012**, *3*, 1730. (e) Popoff, N.; Espinas, J.; Pelletier, J.; Macqueron, B.; Szeto, K. C.; Boyron, O.; Boisson, C.; Del Rosal, I.; Maron, L.; De Mallmann, A.; Gauvin, R. M.; Taoufik, M. *Chem.—Eur. J.* **2013**, *19*, 964.
(19) Herrmann, W. A.; Stumpf, A. W.; Priermeier, T.; Bogdanovic, S.; Dufaud, V.; Basset, J.-M. *Angew. Chem., Int. Ed.* **1996**, *354*, 2803.
(20) Rossi, A. R.; Hoffmann, R. *Inorg. Chem.* **1975**, *14*, 365.
(21) Zhao, Y.; Truhlar, D. G. *Theor. Chem. Acc.* **2008**, *120*, 215.
(22) Feher, F. J.; Blanski, R. L. *Organometallics* **1993**, *12*, 958.
(23) Kozhevnikov, I. V.; Sinnema, A.; Jansen, R. J. J.; van Bekkum, H. *Catal. Lett.* **1994**, *27*, 187.
(24) Bak, M.; Rasmussen, J. T.; Nielsen, N. C. *J. Magn. Reson.* **2000**, *147*, 296.
(25) Bryce, D. L.; Eichele, K.; Wasylishen, R. E. *Inorg. Chem.* **2003**, *42*, 5085.
(26) (a) Scolan, E.; Magnenet, C.; Massiot, D.; Sanchez, C. *J. Mater. Chem.* **1999**, *9*, 2467. (b) Jakobsen, H. J.; Bildsøe, H.; Skibsted, J.; Brorson, M.; Hung, I.; Gan, Z. *Inorg. Chem.* **2011**, *50*, 7676.
(27) Grünert, W.; Feldhaus, R.; Anders, K.; Shpiro, E. S.; Minachev, Kh. *J. Catal.* **1989**, *120*, 444.
(28) Clark, D. N.; Schrock, R. R. *J. Am. Chem. Soc.* **1978**, *100*, 6774.
(29) Frisch, M. J.; Trucks, G. W.; Schlegel, H. B.; Scuseria, G. E.; Robb, M. A.; Cheeseman, J. R.; Montgomery, J. A.; , Jr., Vreven, T.; Kudin, K. N.; Burant, J. C.; Millam, J. M.; Iyengar, S. S.; Tomasi, J.; Barone, V.; Mennucci, B.; Cossi, M.; Scalmani, G.; Rega, N.; Petersson, G. A.; Nakatsuji, H.; Hada, M.; Ehara, M.; Toyota, K.; Fukuda, R.; Hasegawa, J.; Ishida, M.; Nakajima, T.; Honda, Y.; Kitao, O.; Nakai, H.; Klene, M.; Li, X.; Knox, J. E.; Hratchian, H. P.; Cross, J. B.; Bakken, V.; Adamo, C.; Jaramillo, J.; Gomperts, R.; Stratmann, R. E.; Yazyev, O.; Austin, A. J.; Cammi, R.; Pomelli, C.; Ochterski, J. W.; Ayala, P. Y.; Morokuma, K.; Voth, G. A.; Salvador, P.; Dannenberg, J. J.; Zakrzewski, V. G.; Dapprich, S.; Daniels, A. D.; Strain, M. C.; Farkas, O.; Malick, D. K.; Rabuck, A. D.; Raghavachari, K.; Foresman, J. B.; Ortiz, J. V.; Cui, Q.; Baboul, A. G.; Clifford, S.; Cioslowski, J.; Stefanov, B. B.; Liu, G.; Liashenko, A.; Piskorz, P.; Komaromi, I.; Martin, R. L.; Fox, D. J.; Keith, T.; M. A. Al-Laham, Peng, C. Y.; Nanayakkara, A.; Challacombe, M.; Gill, P. M. W.; Johnson, B.; Chen, W.; Wong, M. W.; Gonzalez, C.; Pople, J. A. *Gaussian 03*, Revision B.05; Gaussian Inc.: Wallingford, CT, 2003.
(30) (a) Perdew, J. P. In *Electronic Structure of Solids*; Ziesche, P., Eschrig, H., Eds.; Akademie: Berlin, 1991; Chapter Unified Theory of Exchange and Correlation Beyond the Local Density Approximation. (b) Perdew, J. P.; Burke, K.; Wang, Y. *Phys. Rev. B* **1996**, *54*, 16533–16539. (c) Burke, K.; Perdew, J. P.; Wang, Y. In *Electronic Density Functional Theory: Recent Progress and New Directions*; Dobson, J. F., Vignale, G., Mas, M. P., Eds.; Plenum: New York, 1998; Chapter Derivation of a Generalized Gradient Approximation: the PW91 Density Functional. (d) Perdew, J. P.; Chevary, J. A; Vosko, S. H.; Jackson, K. A.; Pederson, M. R.; Singh, D. J.; Fiolhais, C. *Phys. Rev. B* **1992**, *46*, 6671. (e) Perdew, J. P.; Burke, K.; Wang, Y. *Phys. Rev. B* **1998**, *57*, 14999. (f) Perdew, J. P.; Chevary, J. A.; Vosko, S. H.; Jackson, K. A.; Pederson, M. R.; Singh, D. J.; Fiolhais, C. *Phys. Rev. B* **1993**, *48*, 4978.
(31) Küechle, W.; Dolg, M.; Stoll, H.; Preuss, H. *Mol. Phys.* **1991**, *74*, 1245.
(32) (a) Harihara, P. C.; Pople, J. A. *Theo. Chim. Acta* **1973**, *28*, 213. (b) Hehre, W. J.; Ditchfield, R.; Pople, J. A. *J. Chem. Phys.* **1972**, *56*, 2257.
(33) (a) Davidson, E. R. *Chem. Phys.* **1996**, *260*, 514. (b) Woon, D. E.; Dunning, T. H. *J. Chem. Phys.* **1993**, *98*, 1358.
(34) (a) Wolinski, K.; Hilton, J. F.; Pulay, P. *J. Am. Chem. Soc.* **1990**, *112*, 8251. (b) McWeeny, R. *Phys. Rev.* **1962**, *126*, 1028. (c) London, F. J. *Phys. Radium* **1937**, *8*, 397. (d) Dodds, J. L.; McWeeny, R.; Sadlej, A. J. *Mol. Phys.* **1980**, *41*, 1419. (e) Ditchfield, R. *Mol. Phys.* **1974**, *27*, 789. (f) Junk, P. C.; Steed, J. W. *J. Organomet. Chem.* **1999**, *587*, 191.
(35) (a) Walishen, R. E.; Mooibroek, S.; Macdonald, J. B. *J. Chem. Phys.* **1984**, *81*, 1057. (b) Kongsted, J.; Nielsen, C. B.; Mikkelsen, K. V.; Christiansen, O.; Ruud, K. *J. Chem. Phys.* **2007**, *126*, 034510.
(36) Tosin, G.; Santini, C. C.; Taoufik, M.; De Mallmann, A.; Basset, J. M. *Organometallics* **2006**, *25*, 3324.
(37) Ravel, B.; Newville, M. *J. Synch. Radiat.* **2005**, *12*, 537.
(38) (a) Michalovicz, A. *Logiciels pour la Chimie*; Société Française de Chimie: Paris, 1991; p102. (b) Michalowicz, A.; Moscovici, J.; Muller-Bouvet, D.; Provost, K. *J. Phys.: Conf. Ser.* **2009**, *190*, 012034.
(39) Ankudinov, A. L.; Ravel, B.; Rehr, J. J.; Conradson, S. D. *Phys. Rev. B* **1998**, *58*, 7565.
(40) Reports of the Standards and Criteria Committee of the International XAFS Society 2000: http://ixs.iit.edu/subcommittee_reports/sc/